Nanoscale

MINIREVIEW

View Article Online
View Journal | View Issue

Check for updates

Cite this: *Nanoscale*, 2023, **15**, 13546

Heterostructures of MXenes and transition metal oxides for supercapacitors: an overview

Shagufi Naz Ansari,[a,c] Mohit Saraf, [d] Zahir Abbas[a] and Shaikh M. Mobin *[a,b]

MXenes are a large family of two dimensional (2D) materials with high conductivity, redox activity and compositional diversity that have become front-runners in the materials world for a diverse range of energy storage applications. High-performing supercapacitors require electrode materials with high charge storage capabilities, excellent electrical conductivity for fast electron transfer, and the ability of fast charging/discharging with good cyclability. While MXenes show many of these properties, their energy storage capability is limited by a narrow electrochemically stable potential window due to irreversible oxidation under anodic potentials. Although transition metal oxides (TMOs) are often high-capacity materials with high redox activity, their cyclability and poor rate performance are persistent challenges because of their dissolution in aqueous electrolytes and mediocre conductivity. Forming heterostructures of MXenes with TMOs and using hybrid electrodes is a feasible approach to simultaneously increase the charge storage capacity of MXenes and improve the cyclability and rate performance of oxides. MXenes could also act as conductive substrates for the growth of oxides, which could perform as spacers to stop the aggregation of MXene sheets during charging/discharging and help in improving the supercapacitor performance. Moreover, TMOs could increase the interfacial contact between MXene sheets and help in providing short-diffusion ion channels. Hence, MXene/TMO heterostructures are promising for energy storage. This review summarizes the most recent developments in MXene/oxide heterostructures for supercapacitors and highlights the roles of individual components.

Received 15th April 2023,
Accepted 17th July 2023

DOI: 10.1039/d3nr01755a

rsc.li/nanoscale

1. Introduction

Due to the exhaustion of fossil fuels and subsequent environmental issues, high efficiency energy storage technologies are urgently needed.[1–3] Rechargeable batteries and electrochemical capacitors are considered to be the future of storage technologies.[4–10] Although rechargeable batteries show higher energy densities, they are limited by a low power density and a small cycle life.[11–19] Widespread interest has been developed in supercapacitors due to their superior power density, high cyclability, and high rate charge storage.[20–25]

Supercapacitors, also referred to as ultra-capacitors, are generally categorized into double-layer capacitors and pseudocapacitors on the basis of their elementary charge storage mechanism (Fig. 1).[26] Double-layer capacitors store charge electrostatically by physically adsorbing ions, whereas reversible faradic redox reactions proceed at the surface of electrode materials in pseudocapacitors to store the charge. Hence, a larger amount of charge can be stored in pseudocapacitors, and their energy density is comparatively high.[26,27]

Supercapacitors are constructed with two electrodes, current collectors, an electrolyte, a separator, and other packaging materials.[20–25] The electrochemical performance of supercapacitors primarily relies on the employed materials, electrolytes, and electrode architecture. Recently, 2D nanomaterials, such as graphene,[28] transition metal oxides/hydroxides,[29–31] transition metal dichalcogenides,[32,33] and MXenes,[34,35] have been massively investigated as active materials in energy storage applications. Among them, MXenes have drawn immense attention due to their distinctive characters such as larger interlayer spacing, redox activity, metallic conductivity, and long cyclability.[34,36–44] MXenes are 2D transition metal carbides, nitrides, and/or carbonitrides.[45–47] MXenes have a

---

[a] *Department of Chemistry, Indian Institute of Technology Indore, Simrol, Khandwa Road, Indore 453552, India. E-mail: xray@iiti.ac.in; Tel: +91 731 6603 336*

[b] *Center for Advance Electronics, Indian Institute of Technology Indore, Simrol, Khandwa Road, Indore 453552, India*

[c] *Department of Chemistry, School of Engineering, Presidency University, Bangalore, 560064, India*

[d] *A.J. Drexel Nanomaterials Institute and Department of Materials Science and Engineering, Drexel University, Philadelphia, PA 19104, USA*

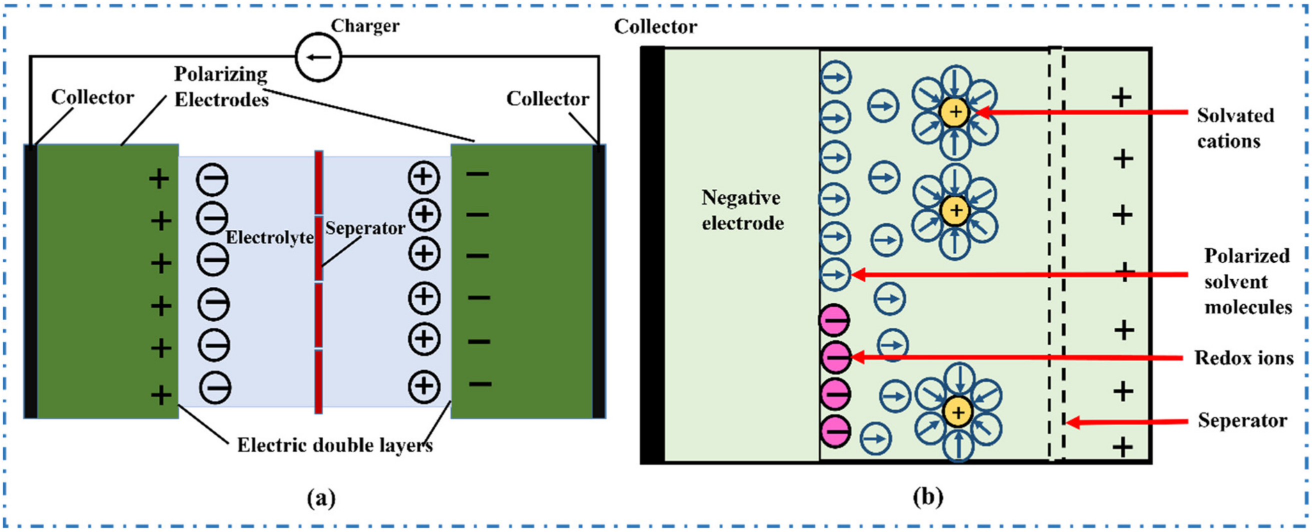

Fig. 1 Mechanism of charge storage in (a) an EDLC (electric double layer capacitor) and (b) pseudocapacitors.[26]

standard formula of $M_{n+1}X_nT_x$, where M represents an early transition metal, X signifies C and/or N, T signifies surface functional groups (*e.g.*, –OH, –F, and –O), and $n = 1, 2, 3$, or 4.[34,36–45] They show outstanding electrochemical properties, due to their inherently conductive carbide core and the possibility of charge transfer due to the presence of transition metals with flexible oxidation numbers.[48–51] Since the discovery of $Ti_3C_2T_x$ MXenes in 2011, several MXenes with unique properties have been synthesized and used as electrode materials for energy storage applications.[34,36–45,52–57]

Despite several suitable properties, MXene electrodes face certain issues during electrochemical testing, such as restacking of MXene sheets and oxidation. Several studies have been reported to address these issues, such as the synthesis of nanostructured MXenes,[58] few-layer MXene sheets,[59] porous MXene architectures,[60] MXene/transition metal chalcogenides (TMCs)[61] and MXene/transition metal oxide (TMO) composites.[62] Particularly, TMOs have gained wide attention thanks to their high redox activity, ease of preparation, controlled shape, and functionality.[63–65] Therefore, hybrid electrodes consisting of MXenes and TMOs can help in achieving high redox reactivity at higher rates with improved cycling efficiency. Furthermore, the volume expansion of TMOs can be minimized and the tendency of MXene sheets to restack can be reduced in these hybrid electrodes.[66–68] Several heterostructures of MXenes and TMOs have been documented through hydrothermal reactions,[69–71] electrostatic self-assembly,[35,72] and *in situ* progression,[73,74] showing unique arrangements and morphologies. Moreover, MXene surface terminations could be systematically directed to reduce the irreversible capacity since the electrochemical properties of MXenes greatly depend on the surface chemistry.[48–51,75–80] This minireview systematically focuses on the formation strategies of such heterostructures and highlights the aspects governing their improved energy storage capability.

2. Synthesis methodologies of MXenes and their heterostructures with TMOs

TMOs can be easily integrated with MXenes using various approaches. The physical and chemical characteristics of the formed heterostructures are directly influenced by their synthesis method. Below, some common methods have been discussed.

2.1 Hydrothermal method

The advantages of the hydrothermal method include high product crystallinity, low operating temperatures, and high diffusion rates. Here, MXenes are dispersed in a liquid phase with a different material under extreme conditions of pressure and heat. Moreover, the functional groups can be controlled on the surface of MXene-based heterostructures, further advancing their activity. In 2018, Yu and coworkers obtained a novel 2D/2D heterojunction of ultrathin Ti_3C_2/Bi_2WO_6 nanosheets through the *in situ* growth of Bi_2WO_6 on the surface of Ti_3C_2 (Fig. 2a–c).[69] For this process, few-layer ultrathin Ti_3C_2 nanosheets were acquired through the ultrasonic exfoliation of multilayered MXenes (Fig. 2a). The negative potential of Ti_3C_2 makes Bi^{3+} ions easily adsorbed on their surface, which results in a close interface between Ti_3C_2 and Bi_2WO_6. The growth of Bi_2WO_6 on the Ti_3C_2 surface is ensured by the electrostatic attraction between Bi^{3+} cations and Ti_3C_2, which leads to strong contact between Ti_3C_2 and Bi_2WO_6. The constructed heterostructure composite is fashioned with abundant atomic layers, a large interface contact area, and a quite small charge transport distance, which potentially improved the photocatalytic efficiency of the heterostructure by 6 times as compared to pristine Bi_2WO_6 nanosheets. In 2019, an innovative ultrafast kinetics net electrode was constructed through

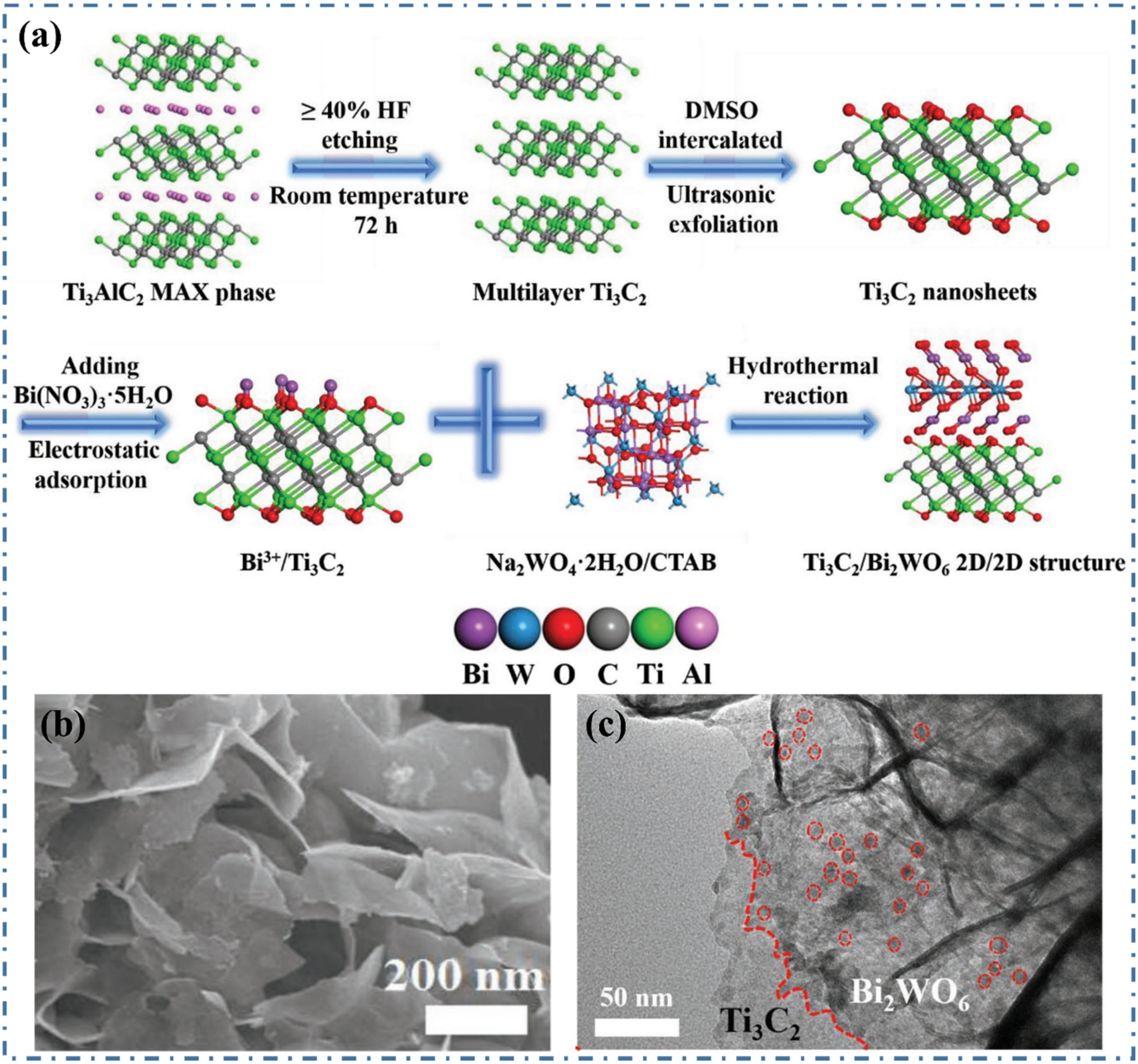

Fig. 2 (a) Schematic demonstration of the synthesis of ultrathin Ti_3C_2/Bi_2WO_6 nanosheets (2D/2D heterojunction). (b and c) FESEM and TEM images of Ti_3C_2/Bi_2WO_6.[69] Reproduced from ref. 69 with permission from Elsevier, copyright 2020.

a $MoSe_2$/MXene heterojunction by Jiang and coworkers using a straightforward hydrothermal process and the thermal annealing method.[70] The prepared heterojunction moderated the volume expansion, improved the low electronic conductivity and polyselenide shuttle effect of $MoSe_2$. In addition to dramatically enhancing the reaction kinetics, the force of van der Waals contact among $MoSe_2$ and MXenes successfully capped the volume shift throughout sodium ion insertion/extraction cycles. The $MoSe_2/Ti_3C_2$ heterojunctions acquired a 3D network with rich porous structure, demonstrating a potential anode with a reversible capacity of 434 mA h g^{-1} for 200 cycles at 1 A g^{-1}. However, MXenes can undergo oxidation by dissolved oxygen in aqueous solutions under hydrothermal conditions.

2.2 Self-assembly strategy

Self-assembly has grown to be the most advanced bottom-up strategy for building nanomaterials in terms of their size and morphology. This strategy is easy to implement, economical, extremely effective, and outcomes in metal-oxide nanostructures packed tightly on MXene nanosheets. Here, metal oxides (MOs) self-assemble on MXenes (Ti_3C_2) through electrostatic interactions, or van der Waals interactions, consequently reducing the surface energy and stabilizing the structure.

The potential of individual components is adequately assimilated in the subsequent MO/MXene heterostructures. Correspondingly, MXene nanosheets serve as a substrate for circumventing the aggregation of TMO nanostructures. Generally, their structures and electrochemical properties are significantly influenced by regulating the proportions of MXenes and the complementary materials. In 2018, Xu and co-workers reported van der Waals interaction-based facile self-assembled nanorods and nanowires of TiO_2 and SnO_2 on MXenes (Ti_3C_2) (Fig. 3a–e).[35] As a substrate, MXene nanosheets were utilized, allowing reversible transportation of electrons and ions at the interface and inhibiting the TMO nanostructures from clumping together. Consequently, TMO nanostructures act as a spacer to block MXene nanosheets from stacking, thus retaining the active sites. MXene nanosheets with outstanding mechanical flexibility improve the pulverization of SnO_2 nanowires, which are known for experiencing extreme volume expansion. In 2021, the same group proposed another ideal and compact interfacial arrangement of Fe_3O_4 and MXenes as a result of the self-assembly process facilitated by van der Waals interactions.[66] The route permits a uniform dispersion of Fe_3O_4 nanodots over MXene nanosheets. In 2023, Guang-Sheng Wang reported a versatile method for the synthesis of Co-based bimetallic oxide heterostructures with a flower shaped morphology, which can be used to build a 3D crossing network structure *via* the electrostatic self-assembly of MXene nanosheets.[72] The built network is practicable for constructing conductive pathways, facilitating the unrestricted movement of electrons. The obtained bimetallic MXene composite demonstrated excellent microwave absorption capacity with a minimum reflection loss. Unlike hydrothermal synthesis, this self-assembly approach does not result in structural deterioration of MXene nanosheets.

2.3 Chemical deposition strategy

With chemical liquid phase deposition, specific coatings can be deposited on the target material *via* controlled chemical reactions. This technique can be used to peel away the inner layers of multilayered MXenes or to coat MXene nanosheets with nanoparticles to avoid restacking. Unnecessary oxidation of MXenes could be avoided here as this method is performed under mild reaction conditions (relatively low pressure and temperature). In 2022, a porous hydrogel with a 3D hierarchical Ti_3C_2TX@NiO–rGO heterostructure was prepared by Haijun Xu, and it demonstrated excellent mechanical properties and conductivity.[81] To synthesize the heterostructure, chemical bath deposition and thermal annealing methods were used, followed by a simple GO-assisted self-convergence hydrothermal process. The heterostructure displayed a 2D arrangement inherently consisting of a thin, wrinkled, and paper-like

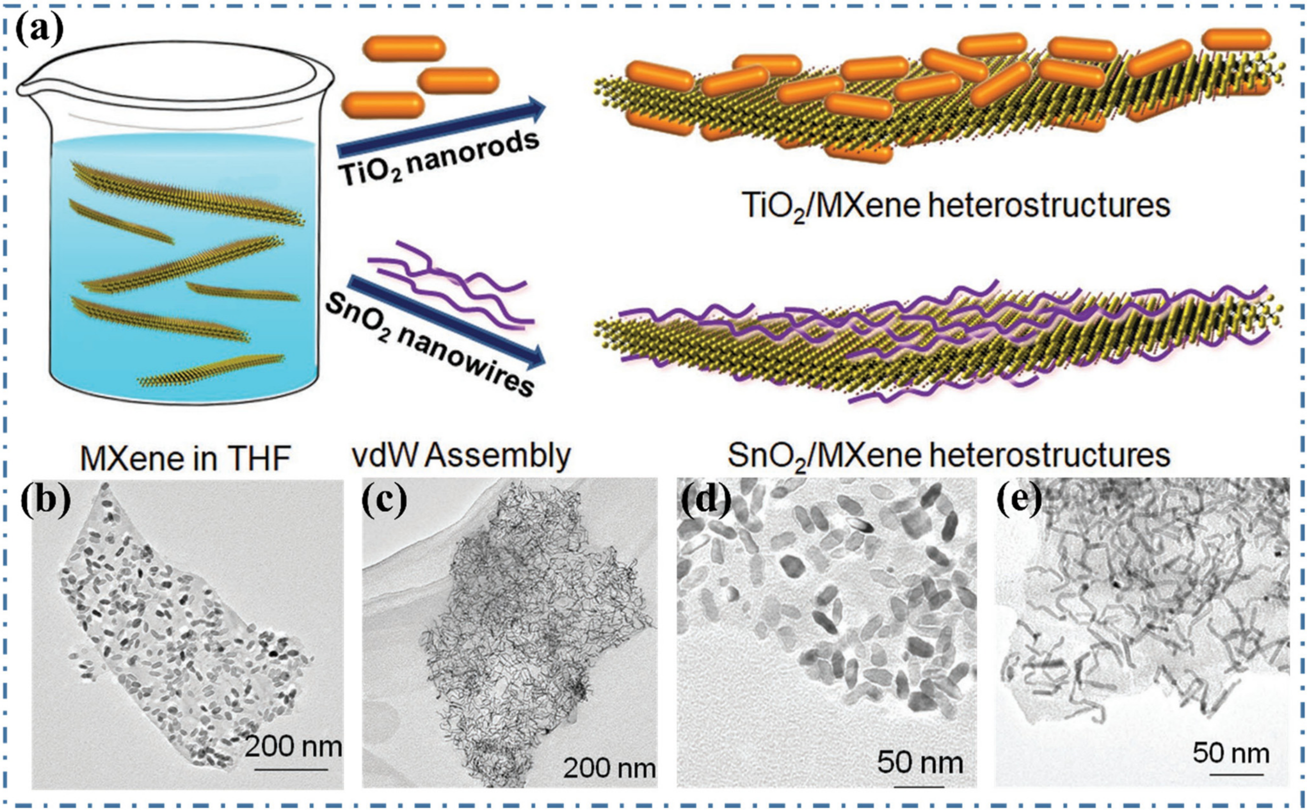

Fig. 3 (a) Schematic illustration for the self-assembly of SnO_2 nanowires and TiO_2 nanorods on the nanosheets of MXenes in THF *via* van der Waals contacts. (b and c) Pictorial representation of the TEM images of TiO_2/MXene heterostructures at various magnification scales. (d and e) TEM images of SnO_2/MXene heterostructures at various magnification scales.[35] Reproduced from ref. 35 with permission from Wiley-VCH, copyright 2018.

composition. A large electroactive surface and rapid ion/electron transport channels were achieved by preparing a 3D mesoporous architecture that efficiently constrained the aggregation of the $Ti_3C_2T_x$@NiO heterostructure. Li *et al.* synthesized RuO_2 nanoparticles that are evenly attached to MXene nanosheets.[47] During the reaction, negatively charged MXene surfaces were electrostatically self-attracted onto positively charged Ru^{3+} surfaces prior to the oxidation of Ru cations, which efficiently hampers the restacking of MXene nanosheets. The increased specific surface area of the mesoporous structure of $RuO_2 \cdot xH_2O$@MXenes might have hastened the electrolyte ion migration and diffusion, further enhancing the electrochemical performance.

2.4 High temperature *in situ* derivation strategy

By heating MXenes with or without additional phases, high-temperature *in situ* derivation is a strategy for creating a second phase on the surface of MXenes.[73] For example, Yang *et al.* established an *in situ* growth of an accordion-like TiO_2/Ti_3C_2 composite and employed it as an anode material for LIBs (lithium-ion batteries) and SIBs (sodium-ion batteries).[73] MXene heterostructures are formed as a result of oxidation, sulfidation, or a phase transition that occurs during the heat treatment. One example is the single-step oxidation of 2D Ti_3C_2 or Nb_2C powders at 1150 °C for 30 s to produce thin sheets of disordered graphitic carbon that are embellished with oxide nanocrystals of anatase or niobia, Nb_2O_5 (Fig. 4a–c).[74] Analogous structures were acquired by oxidizing Ti_3C_2 in CO_2 between 150 and 300 °C. Controlling the process can be challenging with flash oxidation, especially if the particles get on fire. The layers of the as-synthesized $Ti_3C_2T_x$ were analogous to those of exfoliated graphite. During flash oxidation, oxide nanocrystals were shown to form at the edges and between the layers. In another example, a humidity sensor was developed by growing *in situ* TiO_2 nanowires on a 2D Ti_3C_2 MXene using the alkali oxidation process, showing an urchin-like morphology.[82] As compared to pure Ti_3C_2 or pure TiO_2, the sensor's remarkable sensitivity is due to its extraordinarily high specific surface area. OH-terminated Ti_3C_2 sheets are regarded as metallic due to their extremely low band gap and excellent carrier mobility (Fig. 4d–f).[82]

3. Heterostructures of MXenes/TMOs for supercapacitors

Heterostructures of MXenes/TMOs are promising electrode materials in energy storage devices, particularly supercapacitors, which are gaining much attention due to their high power density and high cyclability.[83] In MXene/TMO heterostructures, TMOs prevent the restacking of MXene sheets, while the MXene layers might prevent the accumulation of TMOs and disseminate charge and ion transport thanks to their high electrical conductivity. TMO nanostructures may also serve as spacers to separate the MXene layer, improving interfacial connections and enriching the active sites, leading to a high cyclability of the heterostructures. MXene nanosheets can also serve as conducting substrates for the growth of TMO nanoarchitectures, which helps in enhancing electron transportation.[84] It should be noted that MXene/TMO interfacial bonding can be significantly influenced by the morphological, structural, and surface-controlled functional groups of MXenes and TMOs together.[35,74,81] Thus, MXene/TMO heterostructures are promising electrode materials for supercapacitors due to the synergistic interaction between conductive MXenes and high capacity TMOs.[85,86]

TMOs such as non-layered metal oxides, binary transition metal oxides (BMOs), *e.g.*, MnO_2, SnO_2, $NiMoO_4$, $ZnCo_2O_4$, $NiCoO_4$, *etc.*, are the most suitable choice with MXenes for their high redox capacity.[87–89] When combined with MXenes, manganese oxides (MnO_2) are one of the most extensively researched among all oxides because of their high theoretical specific capacitance value, low toxicity, low cost, and ease of fabrication.[62,90–93] In addition, MnO_2 has a fast redox reaction for improved charge storage ability compared to other materials due to its varying oxidation states from Mn^{3+} to Mn^{4+}. It exists in six crystal phases, which produce a wide range of distinct crystal shapes.[76] In addition to having a high theoretical capacitance of 1370 F g^{-1} and a wide electrochemical window of 0–0.9 V, MnO_2 can also function in mild aqueous electrolytes, leading to less chemical corrosion of the current collector and structural breakdown.[35,74,81] Thus, MnO_2 and MXene hybrids with various morphologies have been extensively studied to produce supercapacitors demonstrating high performance. For example, in 2022 Meng *et al.* explored a heterojunction of MnO_2 nano lamellas (NL) on $Ti_3C_2T_x$ MXene nanosheets (MnO_2 NL/MX) by maintaining the reaction conditions in terms of morphological and structural compositions. The associated mechanisms are as follows: (i) the heterostructure of MnO_2 NL/MX prevents aggregation and restacking that lead to an increase in the active sites and (ii) direct face-to-face contact guarantees robust electrical interactions between MnO_2 and $Ti_3C_2T_x$, which could improve their inherent electrochemical properties and achieve a specific capacitance of 334.3 F g^{-1} at 0.5 A g^{-1} with a cycling retention of 90% after 5000 successive cycles.[62] In addition, various other heterostructures of MnO_2 with MXenes have also been explored for supercapacitors, *e.g.*, ε-MnO_2 nanowhiskers with $Ti_3C_2T_x$ *via* direct chemical synthesis methods that lead to enhanced supercapacitor performance. MnO_2 nanowhiskers in the MXene framework improve the overall cycling performance by 88% after 10 000 cycles by increasing the electrolyte-accessible surface area and contributing pseudocapacitance.[94] While in 2022, Pan *et al.* constructed MXenes with a MoO_3-based hybrid free standing film as the negative electrode and A-CNT/K_x–MnO_2 as the positive electrode *via* introducing a strategy of K^+ ion intercalation that increases ion/electron transport during the galvanostatic charge–discharge process and helps to operate up to 2 V of a wide operating potential window having an energy density of 36.5 W h kg^{-1}.[95] Another strategy of cation and anion intercalation/deintercalation ion mechanisms in $LnMnO_3$(LMO)/$Ti_3C_2T_x$ was observed by Tomar *et al.*

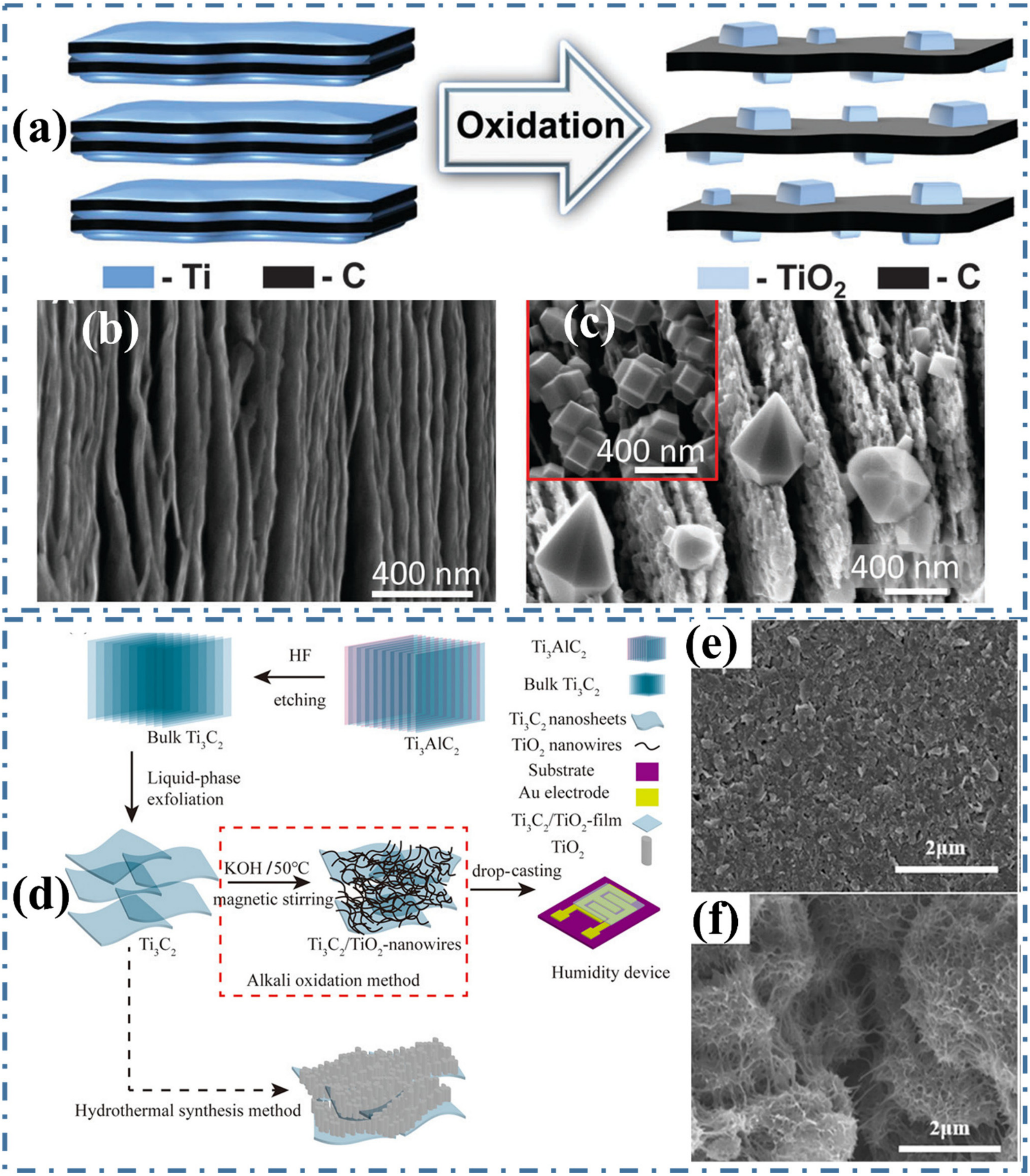

Fig. 4 (a) Diagram showing the oxidation of MXenes, and the creation of a hybrid structure made of graphitic and disordered carbon. (b and c) TEM pictures of $Ti_3C_2T_x$ powders before and after 30 s of flash oxidation in air at 1150 °C.[74] (d) Processes used to prepare the materials including HF etching, LPE, alkali oxidation, and others. SEM images of the (e) initially synthesized 2D-Ti_3C_2 MXene nanosheets and (f) Ti_3C_2/TiO_2 composites that resemble sea urchins.[82] Reproduced from ref. 74 with permission from RSC, copyright 2014; ref. 82 with permission from ACS, copyright 2019.

Here, multilayer MXenes show cations, and oxygen-defective LMOs show anion intercalation. In *ex situ*, XPS analysis found not only K^+ ions but also OH^- ions intercalating into the LMO/$Ti_3C_2T_x$ heterostructures, which increases the charge storage. Furthermore, achieved a specific capacitance of 442.8 F g^{-1} at 3 A g^{-1} with an energy density of 34.1 W h kg^{-1}.[96]

In general, the morphologies and binding mechanisms of MXenes and TMOs are vital for enhancing the supercapacitor performance. It is crucial to ascertain how MXenes and TMOs interact, bind, store energy, transport ions, and interact with one another in order to optimize the performance of supercapacitors.[27,68,97] For surface functionalization and morphological control, Mustafa *et al.* prepared SnO_2 nanoflowers (NFs) treated with ascorbic acid, which activated the surface and served as a linkage for MXene nanosheets in the MXene/SnO_2 heterostructure. SnO_2 NFs served as interlayer spacers and nanopillars to stop restacking, which helped in improving the performance of supercapacitors with 643 F g^{-1} and only 2% degradation loss in cycling stability.[98] In another report, Zhang *et al.* synthesized a heterostructure of $Ti_3C_2T_x$-supported Fe_3O_4 nanoplates (denoted as MXene–Fe) (Fig. 5a–c) *via* a one-step solvothermal strategy as a pseudocapacitive material. The increasing concentration of Fe ions causes hexagonal plates to form and cover the surface of $Ti_3C_2T_x$ uniformly. It acts as a spacer to prevent the $Ti_3C_2T_x$ nanosheets from being stacked again, ensuring there are enough electrochemically active sites. The CV profiles of the MXene–Fe-3 electrode were examined at various scan rates, showing redox peaks indicating the pseudocapacitive feature that leads to determining the electrochemical kinetics and storage mechanism. It has smaller *b* values that lead to more diffusion-controlled behavior (Fig. 6d). At a lower scan rate of 5 mV s^{-1}, the capacitance contribution is only 23.6% (Fig. 6e). With a decrease in diffusive contribution, the capacitive contribution increases with the scan rate (Fig. 6f).[99] Another strategy was employed by Ashraf *et al.* where an ionic liquid (IL)-incorporated delaminated heterostructure, D-Ti_3C_2/MoO_3, was constructed by the integration of imidazolium-based ILs to MoO_3 nanorods that are anchored on the surface of the MXene surface. D-Ti_3C_2 provides structural stability and increases the hydrophilicity of heterostructures, whereas IL@MoO_3 helps in enhancing the electrical conductivity and achieves a capacitance of 1680 F g^{-1} at 1 A g^{-1}.[100]

Liu *et al.* recently prepared a novel class of $W_{18}O_{49}/Ti_3C_2T_x$ pseudocapacitive materials. While both the electrode materials have a negative charge, the electrostatic repulsive force aids in preventing $W_{18}O_{49}$ aggregation and MXene nanosheet's restacking. The heterostructure exhibited a higher supercapacitor performance of 696.2 F g^{-1} at 1 A g^{-1} with a higher cyclic retention of 99.7% after 6000 cycles.[101]

3.1 Binary transition metal oxide (BMO)/MXene heterostructures

Apart from the above-mentioned transition metal oxides, some binary transition metal oxides with MXenes were also explored. Thanks to their multiple oxidation states and the ability to provide abundant active sites for faradic redox reactions, BMOs are able to deliver improved charge storage performance than their single counterparts.[102,103] Zhou *et al.* prepared a $Ti_3C_2T_x$ MXene-wrapped hollow $Co_3V_2O_8$ nanosphere for a

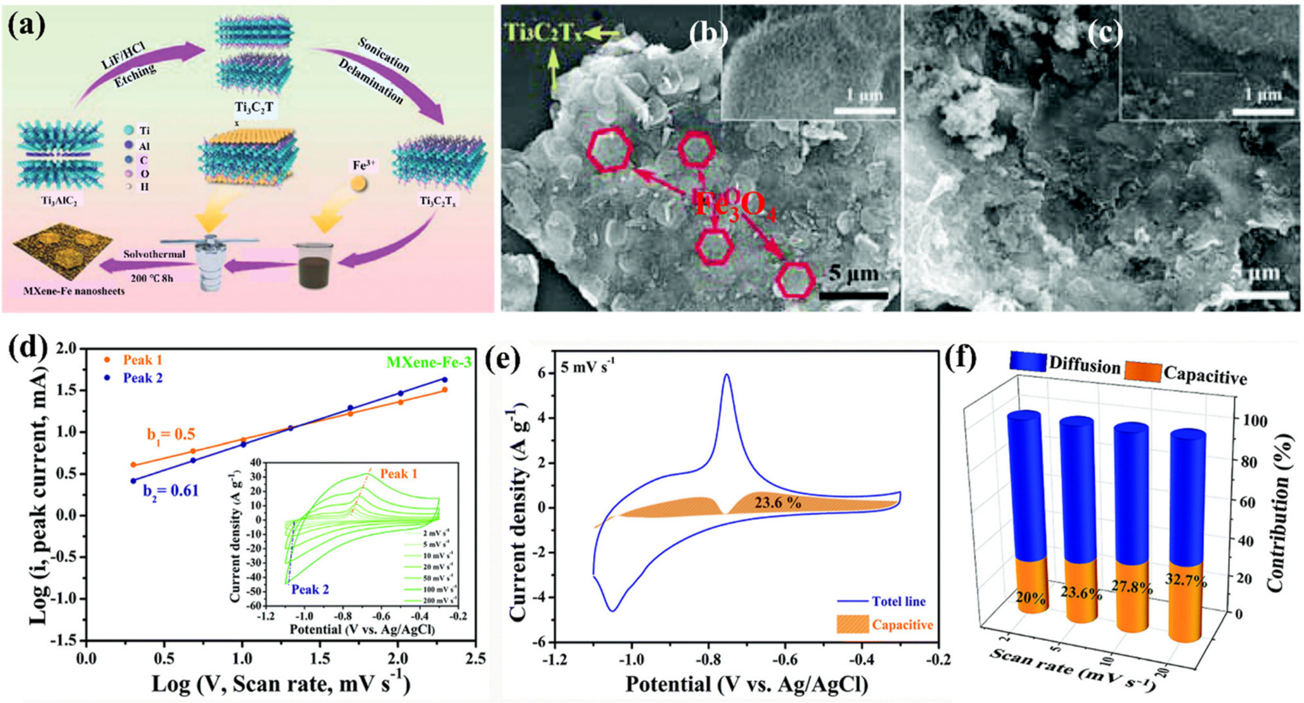

Fig. 5 (a) Schematic illustration of the synthesis of the $Ti_3C_2T_x/Fe_3O_4$ heterostructure. (b and c) SEM images of the heterostructure. (d) Representation of the calculated *b* values of various peak currents, the inset shows the associated CV curves for the MXene-Fe-3 electrode. (e) Capacitive contribution at 5 mV s^{-1}. (f) Capacitive–diffusive contribution at different scan rates.[99] Reproduced from ref. 99 with permission from RSC, copyright 2021.

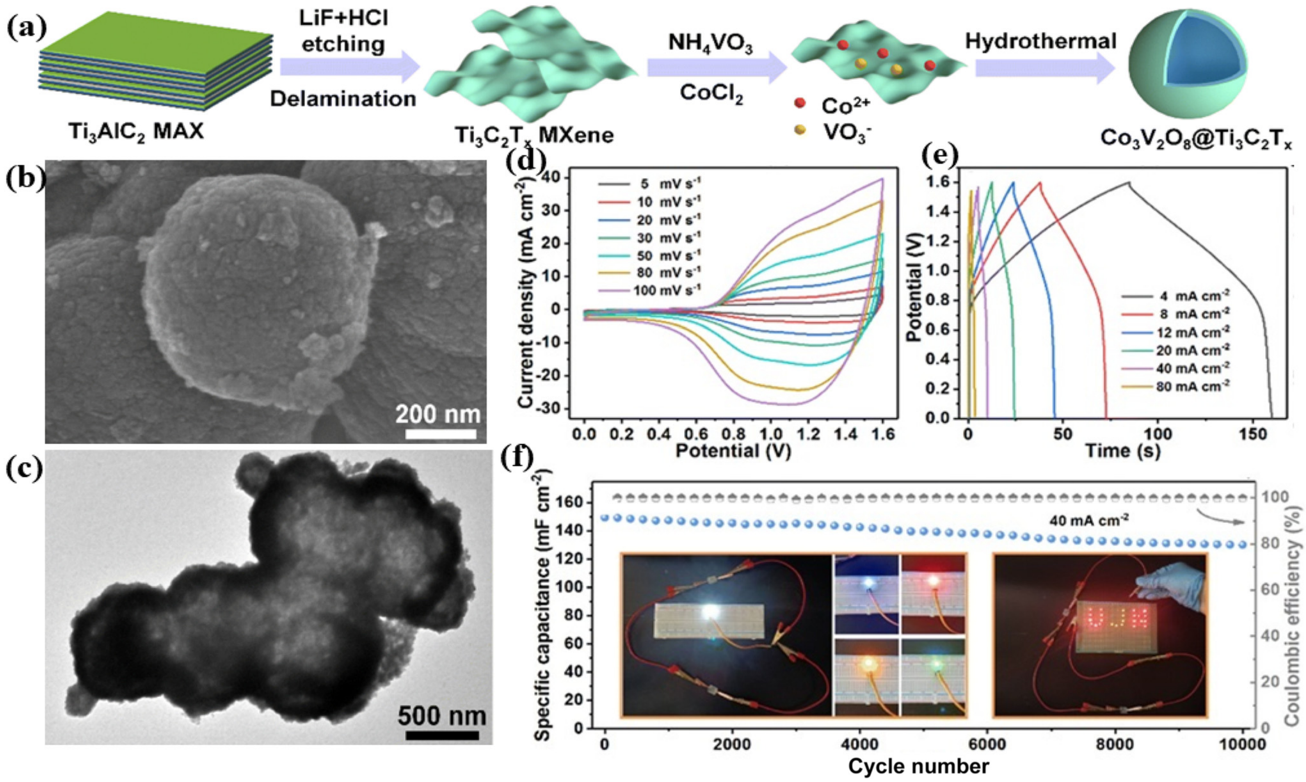

Fig. 6 (a) Representation of the synthesis of a BMO/MXene heterostructure. (b and c) Corresponding SEM and TEM images. (d) CV at various scan rates. (e) GCD at various current densities. (f) Cycling stability, and the insets show photographs of the LED.[104] Reproduced from ref. 104 with permission from RSC, copyright 2022.

solid-state supercapacitor (Fig. 6a). Hollow nanostructures of $Co_3V_2O_8$ nanospheres with an empty interior show in their corresponding SEM and TEM images that they may have enough room to support volume expansion and reduce the mechanical strain brought on by volume change during the repeated charge–discharge process (Fig. 6b and c). This leads to an increase in the areal capacitance of the asymmetric supercapacitor device, which has a higher CV area with different scan rates and a specific capacity varying from 4 to 80 mA cm^{-2}, and at 4 mA cm^{-2} the specific capacity is 203.8 mA cm^{-2} (Fig. 6d and e). The ASC device shows a high cyclic retention of 94.5% after 10 000 successive cycles with the lighting of 25 LED bulbs (Fig. 6f).[104]

Another strategy of electrophoretic deposition was employed by Asen *et al.* to construct a $RuCo_2O_4/Ti_3C_2T_x$ MXene@NF heterostructure. The hierarchical urchin porous structure of $RuCo_2O_4$ grown on $Ti_3C_2T_x$ MXene@NF was confirmed *via* density functional theory studies and the heterostructure shows a remarkable capacitance of 450 F g^{-1} at a current density of 3 A g^{-1} with a high cyclic retention of 94%.[105] In addition to the Ru-based BMO, NiCo, NiMo, and ZnCo, *etc*. were also explored with MXenes for supercapacitors. BMO heterostructure generally follows the same strategy as bare bimetallic oxides for preparing electrode materials for supercapacitors. However, in 2019, Javed *et al.* prepared an all-solid-state flexible ASC device based on a battery-type BMO heterostructure by incorporating $ZnCo_2O_4$ polyhedra on $Ti_3C_2T_x$, which achieved a specific capacitance of 2643.66 F g^{-1} at 2 A g^{-1} with an ultrahigh energy density of 99.94 W h kg^{-1}.[106] Furthermore, the heterostructure was able to achieve higher cycling retention. In 2019, Wang *et al.* reported a facile pathway to prepare hydrophilic $NiMoO_4/Ti_3C_2T_x$ heterostructure nanosheets having interconnected porous construction, enabling the diffusion of electrolyte ions throughout reversible insertion/deinsertion progressions. The selected MXene was made from ultrathin $Ti_3C_2T_x$ flakes that were synthesized by removing Al layers from bulk Ti_3AlC_2, followed by LiF/HCl etching. Subsequently, the negatively charged $Ti_3C_2T_x$ flake's surfaces were electrostatically attached with nickel and molybdenum ions using the hydrothermal process and post-calcination, generating the $NiMoO_4/Ti_3C_2T_x$ heterostructure. The greater hydrophilicity and electrical conductivity of $Ti_3C_2T_x$, as well as the synergistic interactions between $NiMoO_4$ and $Ti_3C_2T_x$, resulted in a high capacitance of 1364 F g^{-1} at 0.5 A g^{-1}. Additionally, an asymmetric supercapacitor with a large 1.6 V potential window and an energy density of 33.76 W h kg^{-1} was achieved by combining a reduced graphene oxide hydrogel as the negative electrode with a $NiMoO_4/Ti_3C_2T_x$ as the positive electrode.[107]

The elasticity and flexibility of MXenes can be reflected in their in-plane stiffness (C) and out-of-plane rigidity (D). The C and D of MXenes are strongly influenced by the M element type, surface functional groups, and MX thickness.[17] MXenes are a type of strong yet flexible material, as evidenced by the Foppl–von Karman numbers per area (C/D), which are equivalent to those of the MoS_2 monolayer.[67] MXenes have D values ranging from 4 to 156 eV, which are quite higher than that of monolayer graphene (1.2 eV), logically concluding that monolayer MXenes have a much higher bending rigidity than monolayer graphene. Interestingly, the bending rigidity of three-atom-thick Ti_2C and Nb_2C MXenes was more flexible than that of three-atom-thick MoS_2 (approximately 9.14 eV). Surface termination in $Ti_{n+1}C_n$ (n = 1, 2, or 3) might prevent the collapse of surface atomic layers and withstand significant stresses under tensile loading, increasing MXenes' mechanical adaptability makes them prime materials for fabricating flexible electrodes and other electronic devices.[17,67] With an increase in layer thickness, MXenes become less flexible. Even though the thinnest MXenes are the most flexible, their in-plane stiffness decreases as their thickness decreases. Moreover, MSC electrodes printed with MXene structures have emerged as a promising option for the development of superior electrochemical performance.[108] According to a study published in 2019, Li *et al.* uniformly anchored hydrous ruthenium oxide (RuO_2) nanoparticles on the as-synthesized $Ti_3C_2T_x$ MXene nanosheets *via* a screen printing process (Fig. 7). The fabricated MSCs had a better volumetric capacitance of 864.2 F cm^{-3} at 1 mV s^{-1}, remarkable cycling stability (90% retention after 10 000 cycles), a virtuous rate capacity of 2000 mV s^{-1}, and wonderful flexibility showing 87.3% retention of the initial capacitance after 2000 bending cycles.[108]

Lithium-ion capacitors (LICs), which fully combine the advantages of LIBs and SCs, often have high power/energy densities and a long lifespan in a single device.[109,110] With much greater theoretical capacities and a minimum rate of volume expansion (~5%) during electrochemical lithiation/delithiation sequences, niobium oxide-based anodes are gaining increasing interest among all TMOs and BMOs. In 2021, for the first time, Qin *et al.* fabricated single-crystalline perovskite $NaNbO_3$ nanocubes (S-P-NNO NCs) by a straightforward hydrothermal alkalization method.[111] Furthermore, the resultant nanocubes were assembled with f-Nb_2CT_x MXenes to construct S-P-NNO/

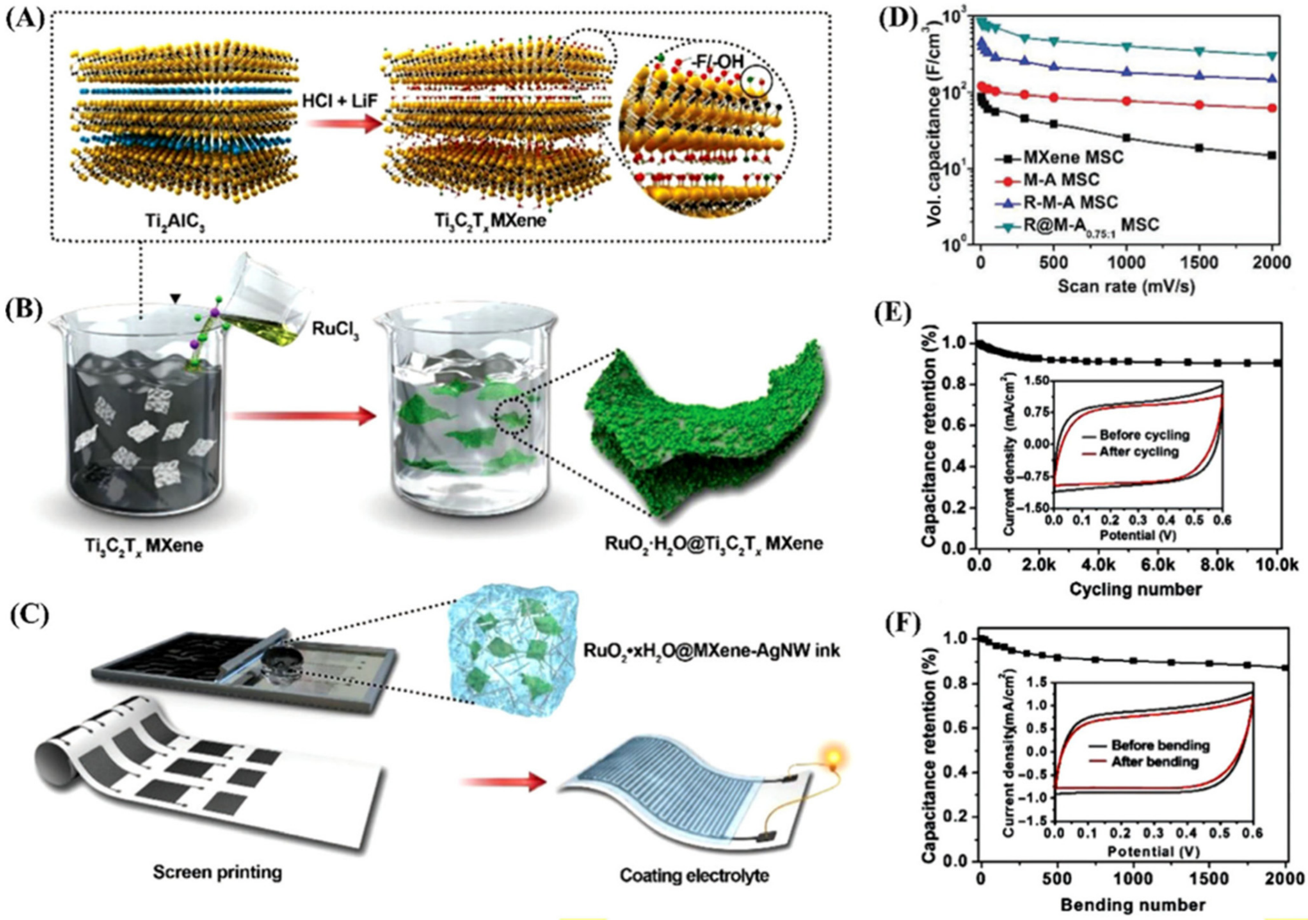

Fig. 7 Illustration of (a) the preparation of $Ti_3C_2T_x$ MXenes; (b) procedure for the synthesis of the $RuO_2·xH_2O$@MXene nanocomposite; (c) development of flexible MSC devices through screen printing; a graphical image showing (d) the volumetric capacitance of various MXene MSCs at diverse scan rates; (e) plot of cycling stability at 100 mV s^{-1} (inset: CV curves recorded before and after cycling); and (f) plot of cycling stability with a bending strain of 5.0% at various bending cycles (the inset shows CV curves recorded before and after 2000 bending cycles at 100 mV s^{-1}).[108] Reproduced from ref. 108 with permission from Wiley-VCH, copyright 2019.

f-Nb_2CT_x heterostructures using a freeze-drying route. The heterostructures were given strong electronic conductivity by the conductive f-Nb_2CT_x MXenes, which also created a three-dimensional (3D) porous network that allowed for quick Li^+ transfer inside the hybrids. Additionally, S-P-NNO NCs distributed equally on and across the nanostructures (NSs) of MXenes, might lessen their tendency to aggregate and self-stack. When used as an anode material for LICs, the produced heterostructures presented excellent pseudocapacitance-dominated capacities and high-rate characteristics because of the synergistic contributions from the S-P-NNO NCs and f-Nb_2CT_x NSs. The assembled asymmetric capacitor from the prepared hybrid demonstrated a high energy density of ~241 W h kg^{-1} at 56 W h kg^{-1} with a superior power density of ~13 kW kg^{-1}. A noteworthy level of cycling stability was also achieved after 4000 charge–discharge cycles.

3.2 Role of electrolytes in TMO/MXene heterostructures

In the past few decades, most studies have focused on H_2SO_4 and less concentrated salt electrolytes for MXene-based heterostructures. In contrast to neutral aqueous electrolytes, H_2SO_4 is neither safe nor environmentally friendly. Further issues with acidic electrolytes are as follows: (i) because of its acidic nature, there is a possibility that the cell would fail due to corrosion and the generation of by-products, (ii) the generation of the hydrogen evolution reaction leads to a short operation potential window, and (iii) because of the usage of H_2SO_4 and low concentration salt electrolytes, the self-discharge rates of the cells are high. Electrolytes, for instance, gels or "water in salts" (WIS) are therefore being taken into consideration. WIS are extremely concentrated electrolytes (salt/water ratio >1) that have drawn a lot of interest because of their steady, high electrochemical stability window (>2 V), slow self-discharge rates, and the high concentration of salt.[112–115]

By taking these aspects into consideration recently, Saraf *et al.* prepared α-MoO_3/Ti_3C_2 heterostructure-based free-standing films with different compositions *via* simple mixing at room temperature without using any binders. Ti_3C_2 MXenes provide mechanical stability and easy synthesis of free-standing films with α-MoO_3. The electrochemical performance shows multiple redox peaks in a water-in-salt electrolyte (19.8 m LiCl), and a wide operating potential of 1.8 V (*vs.* Ag wire).[116] Zheng *et al.* prepared Mn_3O_4 (+ve electrode)/$Ti_3C_2T_z$ (−ve electrode) with high mass loading (10 mg cm^{-2}) and low self-discharge rates in a 14 M LiCl electrolyte, respectively. Subsequent ASC devices showed ultrahigh energy and power density with excellent rate capability and a wide operating potential window of 1.5 V due to the usage of WIS electrolytes.[117] In addition to the LiCl-based electrolytes, Zheng *et al.* utilized a 21 M lithium bis(trifluoromethanesulphonyl)imide (LiTFSI) electrolyte in a $Mo_{1.3}CT_z$ MXene/MnO_2 system. The tertbutyl ammonium intercalated MnO_2/MXene in a very intense electrolyte shows an ultrahigh potential window of 2.5 V and high-rate capability. Another benefit of this electrolyte is slower SD rates than less concentrated electrolytes.[91] Similarly, such MXene/oxide heterostructures should be explored in other electrolytes such as ionic liquids[118] and organic electrolytes[119] to find new electrochemical insights. Table 1 summarizes the electrochemical performance of some state-of-the-art MXene/TMO heterostructure-based supercapacitors.

4. Theoretical aspects of MXene properties

DFT simulations have favored MXene-based materials having pronounced energy storage density, low diffusion barriers, and excellent stability for energy storage applications.[71,132] Modelling and simulations have been used to determine the surface terminating groups in MXenes.[71,133,134] Although the complication of assemblies and formation makes it exceedingly difficult to experimentally determine surface terminal arrangements at the atomic scale, there is still no clear correlation between MXene termination and the synthesis strategy. An effective method for determining the optimum surface structure of MXenes in this situation is a first-principles simu-

Table 1 Reported state-of-the-art MXene/TMO heterostructures and their supercapacitor performance

S. no	Electrode materials	Specific capacitance/areal capacitance ($F g^{-1}/mF cm^{-2}$)	Current density ($A g^{-1}/mV s^{-1}$)	Cycling efficiency	Ref.
1	$Fe_2O_3/Ti_3C_2T_x$ aerogel	182 F g^{-1}	1	81.74% after 10 000 cycles	120
2	$Fe_2O_3/Ti_3C_2T_x$	486.3 F g^{-1}	1	95.7% after 5000 cycles	121
3	MXene/V_2O_5 film	319.1 F g^{-1}	0.5	70.4%, after 5000 cycles	122
4	$Fe_2O_3/Ti_3C_2T_x$	584 F g^{-1}	1	121% after 13 000 cycles	123
5	CoO_x–$NiO/Ti_3C_2T_x$	1960 F g^{-1}	1	90.2% after 8000 cycles	124
6	MoO_3/D-$Ti_3C_2T_x$	545 F g^{-1}	3	90% after 5000 cycles	125
7	$Ti_3C_2T_x/MoO_{3-x}$/PEDOT:PSS	523.0 F g^{-1}	1	95.5% after 5000 cycles	126
8	$Ti_3C_2T_x$/NiCo-LDHs	1207 F g^{-1}	1	93% after 5000 cycles	127
9	$NiCo_2O_4/Ti_3C_2T_x$/rGO	1633 F g^{-1}	1	86.6% after 10 000 cycles	126
10	V_4C_3TX@NiO/rGO	1009.5 F g^{-1}	1	97.45% after 10 000 cycles	128
11	$MnO_2/Ti_3C_2T_x$	130.5 F g^{-1}	1	100% after 1000 cycles	92
12	N–$Ti_3C_2T_x/TiO_2$	918.69 F g^{-1}	5	74.39% after 10 000 cycles	129
13	$Ti_3C_2T_x$/rGO/Fe_3O_4	1250.5 mF cm^{-2}	1	85.8% after 5000 cycles	130
14	$Ti_3C_2T_x$/NiO/rGO	979 F g^{-1}	0.5	95.6% after 10 000 cycles	131
15	MXene–MnO_2–CoNi-LDHs	922 F g^{-1}	1	79% after 4000 cycles	90

lation, *e.g.*, based on DFT.[134,135] Ashton *et al.* used DFT methods to examine how the chemical configuration and hydrogen chemical potential of MXenes with various terminal groups affected their thermodynamic stability, which shows that the majority of possibilities for MXenes are theoretically synthesizable.[136] Several theoretical research studies have conducted to verify the formation of terminations on the surfaces of numerous MXenes. However, the results are far from an accurate representation of the actual situation as dictated by the etching procedures since the whole intricacy of the surface only considers one or two types of T-groups in a symmetric way and more sophisticated simulation methods are still necessary for an accurate match.[137]

The literature has revealed that the most stable MXenes were those with =O and/or –OH terminations because the –F terminal group was easily exchanged by –OH groups, and –OH terminations were changed to –O terminals at high temperatures, and/or metal adsorption operation, which might occur when they were washed and/or kept in water.[138,139] Sang *et al.* used STEM-EELS in a similar way to characterize single layer $Ti_3C_2T_x$ (with a 7.5 : 1 LiF to Ti_3AlC_2 molar ratio in 6 M HCl at 35 °C for 24 hours).[140] The frequency of various point defects and the significance of etchant concentration in defect production were clarified in the monolayer flakes. The effect of defects on the surface chemistry and electrical characteristics of $Ti_3C_2T_x$ was theoretically investigated using *ab initio* molecular dynamics (AIMD) simulations, and it was shown that the conductivity of $Ti_3C_2T_x$ was not affected by the defect concentration.[133,137]

The identification of numerous metal atoms in MXenes significantly increases the variety of potential chemical compositions and the inherent characteristics of MXenes.[138] An organized Cr_2TiAlC_2 MAX phase structure with a Ti atom layer enclosed between outer Cr layers was first identified by Liu *et al.*[141] Later, Anasori *et al*. applied DFT calculations, and it was predicted that the early transition metals M′ and M″ would exist as an immense family of ordered carbides, $M'_2M''C_2$ and $M'_2M''_2C_3$. When compared to the typical single-metal Ti–C-based MXenes, multiple $Mo_2TiC_2T_x$, $Mo_2Ti_2C_3T_x$, and $Cr_2TiC_2T_x$ exhibit different electrochemical behaviors. Due to their reduced symmetry and flexibility in selecting metal atom combinations to customize their electrical characteristics, multiple metal atom MXenes have a wider spectrum of possible features.[142,143]

4.1 Electronic characteristics of MXenes and their heterostructures with metal oxides

By applying DFT calculations, the band structure of terminated MXenes was found to be metallic in nature.[34,45] $Ti_3C_2T_x$ has a greater electrical conductance than graphene (2500 S m^{-1}) according to experimental measurements, reaching 3250 S m^{-1}.[144,145] Khazaei *et al.* further demonstrated through DFT calculations with a few notable exceptions that the MXenes of metal nitrides M_2N (M = Cr, Zr, Ti) and metal carbides M_2C (M = V, Sc, Ti, Cr, Zr, Nb, Ta) with F, O, or OH termination are frequently metallic and non-magnetic. DFT analysis established that only Ti_2C and Zr_2C exhibit instinctive magnetism for the bare M_2C MXene, while the other bare MXenes lack magnetic properties.[146,147] In comparison with a pure metal oxide electrode, the MXene/metal oxide heterostructure offers a larger specific capacitance, greater rate capability, and more stable cycling performance due to its higher electrical conductivity and quicker electron transfer ability according to DFT calculations.[48] The electronic state and electronic structure can be tuned effectively by the hybrid structure, which supports the enhancement of electrochemical performance. For example, in 2023, Zhang *et al.* confirmed the mechanism behind the better electrochemical performance of the NCO/MGA-300 electrode through DFT calculations[48] In this research an assembly of $NiCo_2O_4$ (NCO) microtubes was laid on/into a $Ti_3C_2T_x$ MXene/reduced graphene oxide aerogel (MGA). The NCO/MGA-300 electrode therefore displayed exceptional gravimetric capacitance equivalent to 1633 F g^{-1} at 1 A g^{-1}, and rate performance of 1492 F g^{-1} at 10 A g^{-1}. Additionally, an asymmetric supercapacitor prepared from this heterostructure exhibited consistent electrochemical performance at various compressive pressures of 20%, 40% and 60% following 100 compression–release cycles. The impact of the heterostructure on the kinetics of redox reactions was computed by the adsorption properties of OH^- on the NCO (220)/MXene heterojunction and NCO (220) surfaces. Given that the heterostructure can hold more electrolyte ions due to its reduced adsorption energy (−2.314 eV), the heterostructure favors the kinetics of redox reactions on electrode surfaces. A considerable charge transfer phenomenon was confirmed by the charge density at the NCO (220)/MXene heterointerface, which showed an accumulating tendency near the surface of NCO (220). The same year, Pathak *et al.* established the importance of theoretical perception gained from DFT calculations for a deeper understanding of the charge-storage mechanism including the assessment of the electronic properties and quantum capacitance of the MXene heterostructure ($MnCo_2O_4/Ti_3C_2T_x$).[71] It also provided the details on the interactions between orbitals, the bonding procedure, and the charge transfer capabilities of each electrode material. DFT simulations revealed higher electronic states around the Fermi level in the $MnCo_2O_4/Ti_3C_2T_x$ hybrid structure and improved quantum capacitance, supporting the superior energy storage capability. The $MnCo_2O_4/Ti_3C_2T_x$ hybrid shows a remarkable specific capacitance of 860.22 F g^{-1} at a current density of 2 A g^{-1}.

5. Conclusions and outlook

MXenes are effective choices to overcome the limitations of currently available energy storage technologies, which not only offer great possibilities for supercapacitors and batteries with enhanced storage capabilities, improved cyclability, and fast charging–discharging, but also advance the continuously expanding materials field. Forming heterostructures of MXenes and oxides and using them as single electrodes is perhaps the most feasible way to improve the energy storage capacity of storage devices. The high conductivity of MXenes helps in retaining the redox capacity of oxides at higher rates and improves the cycling efficiency of oxides. Moreover, several studies have reported a suppressed dissolution of oxides in combination with MXenes.[116] Therefore, MXene/oxide heterostructures are certainly effective choices and deserve sincere attention. Below, we highlight some opportunities that can be taken into consideration for future studies.

- The electrochemistry of MXenes is still in its infancy, which needs to be explored in different electrolytes such as organic, ionic liquid, WIS and mixed-ion electrolytes.
- It is important to establish the key electrochemical properties such as electron transfer, conductivity, ionic and charge transport, and capacitance, and different effective ways to exploit the electrochemistry of MXenes with a particular emphasis on mechanistic aspects.
- Combining MXenes and oxides under the optimized conditions is important for improved performance. When compared to single oxides, the electrical conductivity of a binary oxide is twice as high.[102,103] For this reason, preparing hybrid electrodes of MXenes and binary TMOs could be an effective approach.
- One of the major challenges is the identification of the most suitable combinations of MXenes and TMOs for different energy storage devices. Herein, the role of computational prediction and theoretical investigations in pre-selecting the best possible materials is important. These studies are also important to reveal the dynamics of ions confined between the formed heterostructures.[148]
- 3D MXene/TMO heterostructures could be important for energy storage devices. Such heterostructures of various compositions and terminal groups may improve the ion diffusion and reactive sites.[123]
- The scalable production of MXenes and their heterostructures is another challenge and should be taken as an opportunity.
- The moderate energy density of supercapacitors has been a persistent challenge. While MXenes offer high capacitance, their energy density is limited by the electrochemically stable voltage window due to irreversible anodic oxidation. To address this issue, both structural and electrochemical modifications could be helpful in increasing the energy density. Partial oxidation of MXenes to form oxide nanostructures could be a possible strategy to increase the overall capacity of MXene electrodes. Similarly, asymmetric supercapacitors can be designed where MXenes can be employed as negative electrode materials and oxides as positive electrode materials. In this direction, suitable anodes could be selected based on the behaviour of the materials in the chosen electrolytes to pair up with MXene cathodes. Electrolytes play an important role in governing the energy density. Redesigned electrolytes such as WiS and ionic electrolytes usually show a high electrochemically stable voltage window, leading to a high energy density. Hence, there are numerous possibilities to increase the energy density of MXene and oxide based supercapacitors.

There is no denying to the fact that if sincere efforts are made to address the existing issues in the field of 2D materials for energy storage applications, a new era of tuneable and flexible electrochemical devices based on MXene-based technologies is not far away with a better and brighter future. The application of MXenes and their endless heterostructures in flexible and wearable supercapacitors is among hot research areas. It should be noted that the size, composition, shape, texture, thickness and electrode design and architectures play a vital role in energy storage. Therefore, rational design of MXene/oxide heterostructures with improved chemical and electrochemical stability in different electrolyte systems is crucial to obtain a wider electrochemically stable operational working window and enhanced supercapacitor performance.

Conflicts of interest

The authors declare no conflicts of interest to declare.

Acknowledgements

SMM thanks SERB-DST, New Delhi, India (Project CRG/2020/001769), BRNS, Mumbai, India (Project 58/14/17/2020-BRNS/37215), and IIT Indore for the financial support.

References

1 Y. Feng, L. Tao, Z. Zheng, H. Huang and F. Lin, *Energy Storage Mater.*, 2020, **31**, 274–309.
2 J. Liu, H. Mooney, V. Hull, S. J. Davis, J. Gaskell, T. Hertel, J. Lubchenco, K. C. Seto, P. Gleick, C. Kremen and S. Li, *Science*, 2015, **347**, 1258832.
3 M. Elimelech and W. A. Phillip, *Science*, 2011, **333**, 712–717.
4 X. Yuan, F. Ma, L. Zuo, J. Wang, N. Yu, Y. Chen, Y. Zhu, Q. Huang, R. Holze, Y. Wu and T. Van Ree, *Electrochem. Energy Rev.*, 2021, **4**, 1–34.
5 Y. Zhai, Y. Dou, D. Zhao, P. F. Fulvio, R. T. Mayes and S. Dai, *Adv. Mater.*, 2011, **23**, 4828–4850.
6 Z. Zhang, X. Huang, H. Li, Y. Zhao and T. Ma, *Appl. Surf. Sci.*, 2017, **400**, 238–244.
7 H. Wang, C. Zhu, D. Chao, Q. Yan and H. J. Fan, *Adv. Mater.*, 2017, **29**, 1702093.
8 Z. Mao, R. Wang, B. He, J. Jin, Y. Gong and H. Wang, *Small*, 2023, **19**, 2207224.
9 F. Zhang, X. Guo, P. Xiong, J. Zhang, J. Song, K. Yan, X. Gao, H. Liu and G. Wang, *Adv. Energy Mater.*, 2020, **10**, 2000446.
10 S. Wang, S. Zhao, X. Guo and G. Wang, *Adv. Energy Mater.*, 2022, **12**, 2100864.
11 S. Niu, Z. Wang, M. Yu, M. Yu, L. Xiu, S. Wang, X. Wu and J. Qiu, *ACS Nano*, 2018, **12**, 3928–3937.
12 N. Sun, Z. Guan, Y. Liu, Y. Cao, Q. Zhu, H. Liu, Z. Wang, P. Zhang and B. Xu, *Adv. Energy Mater.*, 2019, **9**, 1901351.

13 Y. Zhong, B. Li, S. Li, S. Xu, Z. Pan, Q. Huang, L. Xing, C. Wang and W. Li, *Nano-Micro Lett.*, 2018, **10**, 56.

14 N. Nitta, F. Wu, J. T. Lee and G. Yushin, *Mater. Today*, 2015, **18**, 252–264.

15 A. E. Baumann, X. Han, M. M. Butala and V. S. Thoi, *J. Am. Chem. Soc.*, 2019, **141**, 17891–17899.

16 J. Duan, X. Tang, H. Dai, Y. Yang, W. Wu, X. Wei and Y. Huang, *Electrochem. Energy Rev.*, 2020, **3**, 1–42.

17 F. Wu, J. Maier and Y. Yu, *Chem. Soc. Rev.*, 2020, **49**, 1569–1614.

18 X. Guo, H. Gao, S. Wang, G. Yang, X. Zhang, J. Zhang, H. Liu and G. Wang, *Nano Lett.*, 2022, **22**, 1225–1232.

19 X. Zhu, K. Wang, Y. Xu, G. Zhang, S. Li, C. Li, X. Zhang, X. Sun, X. Ge and Y. Ma, *Energy Storage Mater.*, 2021, **36**, 291–308.

20 A. S. Aricò, P. Bruce, B. Scrosati, J.-M. Tarascon and W. Van Schalkwijk, *Nat. Mater.*, 2005, **4**, 366–377.

21 S. N. Ansari, M. Saraf, A. K. Gupta and S. M. Mobin, *Chem. – Asian J.*, 2019, **14**, 3566–3571.

22 M. Saraf, R. Rajak and S. M. Mobin, *J. Mater. Chem. A*, 2016, **4**, 16432–16445.

23 M. Saraf, K. Natarajan and S. M. Mobin, *ACS Sustainable Chem. Eng.*, 2018, **6**, 10489–10504.

24 K. Natarajan, A. K. Gupta, S. N. Ansari, M. Saraf and S. M. Mobin, *ACS Appl. Mater. Interfaces*, 2019, **11**, 13295–13303.

25 A. Halder, M. Ghosh, A. Khayum M, S. Bera, M. Addicoat, H. S. Sasmal, S. Karak, S. Kurungot and R. Banerjee, *J. Am. Chem. Soc.*, 2018, **140**, 10941–10945.

26 M. R. Lukatskaya, S. Kota, Z. Lin, M.-Q. Zhao, N. Shpigel, M. D. Levi, J. Halim, P.-L. Taberna, M. W. Barsoum, P. Simon and Y. Gogotsi, *Nat. Energy*, 2017, **2**, 17105.

27 Y. Zhou, K. Maleski, B. Anasori, J. O. Thostenson, Y. Pang, Y. Feng, K. Zeng, C. B. Parker, S. Zauscher, Y. Gogotsi, J. T. Glass and C. Cao, *ACS Nano*, 2020, **14**, 3576–3586.

28 M. D. Stoller, S. Park, Y. Zhu, J. An and R. S. Ruoff, *Nano Lett.*, 2008, **8**, 3498–3502.

29 P. He, H. Yu, D. Li and H. Zhou, *J. Mater. Chem.*, 2012, **22**, 3680.

30 K. Kubota, N. Yabuuchi, H. Yoshida, M. Dahbi and S. Komaba, *MRS Bull.*, 2014, **39**, 416–422.

31 D. Kim, S.-H. Kang, M. Slater, S. Rood, J. T. Vaughey, N. Karan, M. Balasubramanian and C. S. Johnson, *Adv. Energy Mater.*, 2011, **1**, 333–336.

32 M. Chhowalla, H. S. Shin, G. Eda, L.-J. Li, K. P. Loh and H. Zhang, *Nat. Chem.*, 2013, **5**, 263–275.

33 M. Pumera, Z. Sofer and A. Ambrosi, *J. Mater. Chem. A*, 2014, **2**, 8981–8987.

34 M. Naguib, V. N. Mochalin, M. W. Barsoum and Y. Gogotsi, *Adv. Mater.*, 2014, **26**, 992–1005.

35 Y.-T. Liu, P. Zhang, N. Sun, B. Anasori, Q.-Z. Zhu, H. Liu, Y. Gogotsi and B. Xu, *Adv. Mater.*, 2018, **30**, 1707334.

36 M. R. Lukatskaya, O. Mashtalir, C. E. Ren, Y. Dall'Agnese, P. Rozier, P. L. Taberna, M. Naguib, P. Simon, M. W. Barsoum and Y. Gogotsi, *Science*, 2013, **341**, 1502–1505.

37 Y. Xia, T. S. Mathis, M.-Q. Zhao, B. Anasori, A. Dang, Z. Zhou, H. Cho, Y. Gogotsi and S. Yang, *Nature*, 2018, **557**, 409–412.

38 M.-Q. Zhao, C. E. Ren, Z. Ling, M. R. Lukatskaya, C. Zhang, K. L. Van Aken, M. W. Barsoum and Y. Gogotsi, *Adv. Mater.*, 2015, **27**, 339–345.

39 O. Mashtalir, M. R. Lukatskaya, M.-Q. Zhao, M. W. Barsoum and Y. Gogotsi, *Adv. Mater.*, 2015, **27**, 3501–3506.

40 M. Naguib, J. Halim, J. Lu, K. M. Cook, L. Hultman, Y. Gogotsi and M. W. Barsoum, *J. Am. Chem. Soc.*, 2013, **135**, 15966–15969.

41 X. Liang, Y. Rangom, C. Y. Kwok, Q. Pang and L. F. Nazar, *Adv. Mater.*, 2017, **29**, 1603040.

42 X. Liang, A. Garsuch and L. F. Nazar, *Angew. Chem., Int. Ed.*, 2015, **54**, 3907–3911.

43 D. Er, J. Li, M. Naguib, Y. Gogotsi and V. B. Shenoy, *ACS Appl. Mater. Interfaces*, 2014, **6**, 11173–11179.

44 M. Zhao, X. Xie, C. E. Ren, T. Makaryan, B. Anasori, G. Wang and Y. Gogotsi, *Adv. Mater.*, 2017, **29**, 1702410.

45 M. Naguib, M. Kurtoglu, V. Presser, J. Lu, J. Niu, M. Heon, L. Hultman, Y. Gogotsi and M. W. Barsoum, *Adv. Mater.*, 2011, **23**, 4248–4253.

46 M. Saraf, T. Zhang, T. Averianov, C. E. Shuck, R. W. Lord, E. Pomerantseva and Y. Gogotsi, *Small Methods*, 2023, 2201551.

47 X. Li, Z. Huang, C. E. Shuck, G. Liang, Y. Gogotsi and C. Zhi, *Nat. Rev. Chem.*, 2022, **6**, 389–404.

48 M. Zhang, D. Jiang, F. Jin, Y. Sun, J. Wang, M. Jiang, J. Cao, B. Zhang and J. Liu, *J. Colloid Interface Sci.*, 2023, **636**, 204–215.

49 R. A. Chavan, D. M. Ulisso, A. S. Rasal, J. Y. Chang and A. V. Ghule, *Mater. Adv.*, 2023, **4**, 2659–2666.

50 S. De, S. Acharya, C. K. Maity and G. C. Nayak, *ACS Appl. Energy Mater.*, 2023, **6**, 969–980.

51 R. A. Chavan, G. P. Kamble, S. B. Dhavale, A. S. Rasal, S. S. Kolekar, J.-Y. Chang and A. V. Ghule, *Energy Fuels*, 2023, **37**, 4658–4670.

52 Y. Zhong, X. Xia, F. Shi, J. Zhan, J. Tu and H. J. Fan, *Adv. Sci.*, 2016, **3**, 1500286.

53 B. Anasori, M. R. Lukatskaya and Y. Gogotsi, *Nat. Rev. Mater.*, 2017, **2**, 16098.

54 B. Mendoza-Sánchez and Y. Gogotsi, *Adv. Mater.*, 2016, **28**, 6104–6135.

55 X. Xie, Z. Ao, D. Su, J. Zhang and G. Wang, *Adv. Funct. Mater.*, 2015, **25**, 1393–1403.

56 E. G. Da Silveira Firmiano, A. C. Rabelo, C. J. Dalmaschio, A. N. Pinheiro, E. C. Pereira, W. H. Schreiner and E. R. Leite, *Adv. Energy Mater.*, 2014, **4**, 1301380.

57 C. Zhao, X. Wang, J. Kong, J. M. Ang, P. S. Lee, Z. Liu and X. Lu, *ACS Appl. Mater. Interfaces*, 2016, **8**, 2372–2379.

58 Y. Wang, X. Wang, X. Li, Y. Bai, H. Xiao, Y. Liu, R. Liu and G. Yuan, *Adv. Funct. Mater.*, 2019, **29**, 1900326.

59 C. Yu, Y. Gong, R. Chen, M. Zhang, J. Zhou, J. An, F. Lv, S. Guo and G. Sun, *Small*, 2018, **14**, 1801203.

60 S. Abdolhosseinzadeh, J. Heier and C. (John) Zhang, *ChemElectroChem*, 2021, **8**, 1911–1917.

61 X. Chen, S. Wang, J. Shi, X. Du, Q. Cheng, R. Xue, Q. Wang, M. Wang, L. Ruan and W. Zeng, *Adv. Mater. Interfaces*, 2019, **6**, 1901160.

62 W. Meng, J. Zhou, G. Wang, J. Qin, L. Yang, H. Huang, Y. Zhao and H. He, *J. Energy Storage*, 2022, **56**, 106105.

63 S. Fang, D. Bresser and S. Passerini, *Adv. Energy Mater.*, 2020, **10**, 1902485.

64 S. Yuan, X. Duan, J. Liu, Y. Ye, F. Lv, T. Liu, Q. Wang and X. Zhang, *Energy Storage Mater.*, 2021, **42**, 317–369.

65 W.-B. Yu, Z.-Y. Hu, J. Jin, M. Yi, M. Yan, Y. Li, H.-E. Wang, H.-X. Gao, L.-Q. Mai, T. Hasan, B.-X. Xu, D.-L. Peng, G. Van Tendeloo and B.-L. Su, *Natl. Sci. Rev.*, 2020, **7**, 1046–1058.

66 P. Zhang, N. Sun, R. A. Soomro, S. Yue, Q. Zhu and B. Xu, *ACS Appl. Energy Mater.*, 2021, **4**, 11844–11853.

67 R. Li, X. Ma, J. Li, J. Cao, H. Gao, T. Li, X. Zhang, L. Wang, Q. Zhang, G. Wang, C. Hou, Y. Li, T. Palacios, Y. Lin, H. Wang and X. Ling, *Nat. Commun.*, 2021, **12**, 1587.

68 X. Liu, F. Xu, Z. Li, Z. Liu, W. Yang, Y. Zhang, H. Fan and H. Y. Yang, *Coord. Chem. Rev.*, 2022, **464**, 214544.

69 S. Cao, B. Shen, T. Tong, J. Fu and J. Yu, *Adv. Funct. Mater.*, 2018, **28**, 1800136.

70 E. Xu, Y. Zhang, H. Wang, Z. Zhu, J. Quan, Y. Chang, P. Li, D. Yu and Y. Jiang, *Chem. Eng. J.*, 2020, **385**, 123839.

71 M. Pathak, P. Mane, B. Chakraborty and C. S. Rout, *J. Energy Storage*, 2023, **66**, 107475.

72 H.-Y. Wang, X.-B. Sun, Y. Xin, S.-H. Yang, P.-F. Hu and G.-S. Wang, *J. Mater. Sci. Technol.*, 2023, **134**, 132–141.

73 C. Yang, Y. Liu, X. Sun, Y. Zhang, L. Hou, Q. Zhang and C. Yuan, *Electrochim. Acta*, 2018, **271**, 165–172.

74 M. Naguib, O. Mashtalir, M. R. Lukatskaya, B. Dyatkin, C. Zhang, V. Presser, Y. Gogotsi and M. W. Barsoum, *Chem. Commun.*, 2014, **50**, 7420–7423.

75 N. M. Caffrey, *Nanoscale*, 2018, **10**, 13520–13530.

76 H.-W. Wang, M. Naguib, K. Page, D. J. Wesolowski and Y. Gogotsi, *Chem. Mater.*, 2016, **28**, 349–359.

77 L. H. Karlsson, J. Birch, J. Halim, M. W. Barsoum and P. O. Å. Persson, *Nano Lett.*, 2015, **15**, 4955–4960.

78 F. Liu, J. Zhou, S. Wang, B. Wang, C. Shen, L. Wang, Q. Hu, Q. Huang and A. Zhou, *J. Electrochem. Soc.*, 2017, **164**, A709–A713.

79 B. B. Sahoo, V. S. Pandey, A. S. Dogonchi, P. K. Mohapatra, D. N. Thatoi, N. Nayak and M. K. Nayak, *J. Energy Storage*, 2023, **65**, 107335.

80 R. S. Karmur, D. Gogoi, A. Biswas, C. Prathibha, M. R. Das and N. N. Ghosh, *Appl. Surf. Sci.*, 2023, **623**, 157042.

81 W. Chen, Y. Peng, Z. Qiu, X. Zhang and H. Xu, *J. Alloys Compd.*, 2022, **901**, 163614.

82 N. Li, Y. Jiang, C. Zhou, Y. Xiao, B. Meng, Z. Wang, D. Huang, C. Xing and Z. Peng, *ACS Appl. Mater. Interfaces*, 2019, **11**, 38116–38125.

83 M. S. Javed, A. Mateen, I. Hussain, A. Ahmad, M. Mubashir, S. Khan, M. A. Assiri, S. M. Eldin, S. S. A. Shah and W. Han, *Energy Storage Mater.*, 2022, **53**, 827–872.

84 W. Xi, J. Jin, Y. Zhang, R. Wang, Y. Gong, B. He and H. Wang, *Nanoscale*, 2022, **14**, 11923–11944.

85 X. Hui, X. Ge, R. Zhao, Z. Li and L. Yin, *Adv. Funct. Mater.*, 2020, **30**, 2005190.

86 K. Nasrin, V. Sudharshan, K. Subramani and M. Sathish, *Adv. Funct. Mater.*, 2022, **32**, 2110267.

87 X. Dong, Y. Zhang, B. Ding, X. Hao, H. Dou and X. Zhang, *J. Power Sources*, 2018, **390**, 208–214.

88 N. Mahmood, I. A. De Castro, K. Pramoda, K. Khoshmanesh, S. K. Bhargava and K. Kalantar-Zadeh, *Energy Storage Mater.*, 2019, **16**, 455–480.

89 S. T. Mahmud, M. M. Hasan, S. Bain, S. T. Rahman, M. Rhaman, M. M. Hossain and M. Ordu, *ACS Mater. Lett.*, 2022, **4**, 1174–1206.

90 X. Li, Z. Lin, Y. Wei, W. Luo, J. Ding, T. Li and Y. Ma, *J. Energy Storage*, 2022, **55**, 105668.

91 W. Zheng, J. Halim, L. Yang, H. O. Badr, Z. Sun, P. O. Å. Persson, J. Rosen and M. W. Barsoum, *Batteries Supercaps*, 2022, **5**(10), e202200151.

92 H. Jiang, Z. Wang, Q. Yang, M. Hanif, Z. Wang, L. Dong and M. Dong, *Electrochim. Acta*, 2018, **290**, 695–703.

93 Y. Wei, M. Zheng, W. Luo, B. Dai, J. Ren, M. Ma, T. Li and Y. Ma, *J. Energy Storage*, 2022, **45**, 103715.

94 R. B. Rakhi, B. Ahmed, D. Anjum and H. N. Alshareef, *ACS Appl. Mater. Interfaces*, 2016, **8**, 18806–18814.

95 Z. Pan, C. Yang, Y. Li, X. Hu and X. Ji, *Chem. Eng. J.*, 2022, **428**, 131138.

96 A. K. Tomar, T. Kshetri, N. H. Kim and J. H. Lee, *Energy Storage Mater.*, 2022, **50**, 86–95.

97 S. Feng, X. Wang, M. Wang, C. Bai, S. Cao and D. Kong, *Nano Lett.*, 2021, **21**, 7561–7568.

98 H. Mustafa, A. Rasheed, S. Ajmal, N. Sarwar, U. Falak, S. G. Lee and A. Sattar, *Energy Fuels*, 2023, **37**, 2410–2419.

99 L. Zhang, Z. Wang, W. Chen, R. Yuan, K. Zhan, M. Zhu, J. Yang and B. Zhao, *Nanoscale*, 2021, **13**, 15343–15351.

100 I. Ashraf, S. Ahmad, D. Dastan, C. Wang, H. Garmestani and M. Iqbal, *Electrochim. Acta*, 2022, **429**, 141036.

101 S. Liu, T. Zeng, Y. Zhang, Q. Wan and N. Yang, *Small*, 2022, **18**, 2204829.

102 A. M. Patil, N. Kitiphatpiboon, X. An, X. Hao, S. Li, X. Hao, A. Abudula and G. Guan, *ACS Appl. Mater. Interfaces*, 2020, **12**, 52749–52762.

103 J. Yu, Z. Cui, X. Li, D. Chen, J. Ji, Q. Zhang, J. Sui, L. Yu and L. Dong, *J. Energy Storage*, 2020, **27**, 101165.

104 J. Zhou, B. Liu, L. Zhang, Q. Li, C. Xu and H. Liu, *J. Mater. Chem. A*, 2022, **10**, 24896–24904.

105 P. Asen, A. Esfandiar and H. Mehdipour, *Nanoscale*, 2022, **14**, 1347–1362.

106 M. S. Javed, H. Lei, H. U. Shah, S. Asim, R. Raza and W. Mai, *J. Mater. Chem. A*, 2019, **7**, 24543–24556.

107 Y. Wang, J. Sun, X. Qian, Y. Zhang, L. Yu, R. Niu, H. Zhao and J. Zhu, *J. Power Sources*, 2019, **414**, 540–546.

108 H. Li, X. Li, J. Liang and Y. Chen, *Adv. Energy Mater.*, 2019, **9**, 1970050.

109 H. Huang, X. Wang, E. Tervoort, G. Zeng, T. Liu, X. Chen, A. Sologubenko and M. Niederberger, *ACS Nano*, 2018, **12**, 2753–2763.

110 L. Qin, S. Zhu, C. Cheng, D. Wu, G. Wang, L. Hou and C. Yuan, *Small*, 2022, **18**, 2107987.

111 L. Qin, Y. Liu, S. Zhu, D. Wu, G. Wang, J. Zhang, Y. Wang, L. Hou and C. Yuan, *J. Mater. Chem. A*, 2021, **9**, 20405–20416.

112 Q. Zhang, J. Rong, D. Ma and B. Wei, *Energy Environ. Sci.*, 2011, **4**, 2152.

113 M. Xia, J. Nie, Z. Zhang, X. Lu and Z. L. Wang, *Nano Energy*, 2018, **47**, 43–50.

114 L. Xiao, Z. Hu, Y. He, L. Jiao, L. Lv, Q. Yin, Q. Wei, Z. Li and Y. Yang, *ACS Appl. Energy Mater.*, 2023, **6**, 68–78.

115 Z. Wang, Z. Xu, H. Huang, X. Chu, Y. Xie, D. Xiong, C. Yan, H. Zhao, H. Zhang and W. Yang, *ACS Nano*, 2020, **14**, 4916–4924.

116 M. Saraf, C. E. Shuck, N. Norouzi, K. Matthews, A. Inman, T. Zhang, E. Pomerantseva and Y. Gogotsi, *Energy Environ. Mater.*, 2023, e12516.

117 W. Zheng, J. Halim, Z. Sun, J. Rosen and M. W. Barsoum, *Energy Storage Mater.*, 2021, **38**, 438–446.

118 G. Valurouthu, R. Panigrahi, M. Saraf, C. E. Shuck, B. S. Mallik, N. Kurra and Y. Gogotsi, *Batteries Supercaps*, 2023, **6**, e202300009.

119 J. Li, X. Wang, W. Sun, K. Maleski, C. E. Shuck, K. Li, P. Urbankowski, K. Hantanasirisakul, X. Wang, P. Kent, H. Wang and Y. Gogotsi, *ChemElectroChem*, 2021, **8**, 151–156.

120 Y. Luo, Y. Tang, X. Bin, C. Xia and W. Que, *Small*, 2022, **18**, 2204917.

121 T.-Z. Shi, Y.-L. Feng, T. Peng and B.-G. Yuan, *Electrochim. Acta*, 2021, **381**, 138245.

122 W. Luo, Y. Sun, Z. Lin, X. Li, Y. Han, J. Ding, T. Li, C. Hou and Y. Ma, *J. Energy Storage*, 2023, **62**, 106807.

123 Y. Ma, H. Sheng, W. Dou, Q. Su, J. Zhou, E. Xie and W. Lan, *ACS Appl. Mater. Interfaces*, 2020, **12**, 41410–41418.

124 X. Zhang, B. Shao, A. Guo, Z. Gao, Y. Qin, C. Zhang, F. Cui and X. Yang, *J. Alloys Compd.*, 2021, **862**, 158546.

125 Y. Wang, X. Wang, X. Li, R. Liu, Y. Bai, H. Xiao, Y. Liu and G. Yuan, *Nano-Micro Lett.*, 2020, **12**, 115.

126 P. Zhang, Y. Sui, W. Ma, N. Duan, Q. Liu, B. Zhang, H. Niu and C. Qin, *Dalton Trans.*, 2023, **52**, 710–720.

127 X. Wu, B. Huang, Q. Wang and Y. Wang, *Chem. Eng. J.*, 2020, **380**, 122456.

128 W. Chen, Z. Geng, S. Zhu, Z. Qiu, X. Zhang and H. Xu, *Sustainable Energy Fuels*, 2022, **6**, 4938–4947.

129 J. Yu, M. Zeng, J. Zhou, H. Chen, G. Cong, H. Liu, M. Ji, C. Zhu and J. Xu, *Chem. Eng. J.*, 2021, **426**, 130765.

130 L. Zhang, K. Yu, Y. Li, Z. Wang, K. Zhan, J. Yang and B. Zhao, *ACS Appl. Nano Mater.*, 2023, **6**, 482–491.

131 W. Chen, C. Hao, Z. Qiu, X. Zhang, H. Xu, B. Yu and S. Chen, *ACS Appl. Mater. Interfaces*, 2022, **14**, 19534–19546.

132 H. Zhu, Z. Liang, S. Xue, X. Ren, X. Liang, W. Xiong, L. Gao and A. Liu, *Ceram. Int.*, 2022, **48**, 27217–27239.

133 V. M. Hong Ng, H. Huang, K. Zhou, P. S. Lee, W. Que, J. Z. Xu and L. B. Kong, *J. Mater. Chem. A*, 2017, **5**, 3039–3068.

134 Y. Bai, K. Zhou, N. Srikanth, J. H. L. Pang, X. He and R. Wang, *RSC Adv.*, 2016, **6**, 35731–35739.

135 C. Zhan, W. Sun, Y. Xie, D. Jiang and P. R. C. Kent, *ACS Appl. Mater. Interfaces*, 2019, **11**, 24885–24905.

136 M. Ashton, N. Trometer, K. Mathew, J. Suntivich, C. Freysoldt, S. B. Sinnott and R. G. Hennig, *J. Phys. Chem. C*, 2019, **123**, 3180–3187.

137 X. Sang, Y. Xie, M.-W. Lin, M. Alhabeb, K. L. Van Aken, Y. Gogotsi, P. R. C. Kent, K. Xiao and R. R. Unocic, *ACS Nano*, 2016, **10**, 9193–9200.

138 J. L. Hart, K. Hantanasirisakul, A. C. Lang, B. Anasori, D. Pinto, Y. Pivak, J. T. Van Omme, S. J. May, Y. Gogotsi and M. L. Taheri, *Nat. Commun.*, 2019, **10**, 522.

139 T. Bashir, S. A. Ismail, J. Wang, W. Zhu, J. Zhao and L. Gao, *J. Energy Chem.*, 2023, **76**, 90–104.

140 X. Sang, Y. Xie, D. E. Yilmaz, R. Lotfi, M. Alhabeb, A. Ostadhossein, B. Anasori, W. Sun, X. Li, K. Xiao, P. R. C. Kent, A. C. T. Van Duin, Y. Gogotsi and R. R. Unocic, *Nat. Commun.*, 2018, **9**, 2266.

141 Z. Liu, L. Zheng, L. Sun, Y. Qian, J. Wang and M. Li, *J. Am. Ceram. Soc.*, 2014, **97**, 67–69.

142 Y. Gogotsi and B. Anasori, *ACS Nano*, 2019, **13**, 8491–8494.

143 J. Wang, W. Liu, G. Luo, Z. Li, C. Zhao, H. Zhang, M. Zhu, Q. Xu, X. Wang, C. Zhao, Y. Qu, Z. Yang, T. Yao, Y. Li, Y. Lin, Y. Wu and Y. Li, *Energy Environ. Sci.*, 2018, **11**, 3375–3379.

144 S. J. Kim, H.-J. Koh, C. E. Ren, O. Kwon, K. Maleski, S.-Y. Cho, B. Anasori, C.-K. Kim, Y.-K. Choi, J. Kim, Y. Gogotsi and H.-T. Jung, *ACS Nano*, 2018, **12**, 986–993.

145 S. Stankovich, D. A. Dikin, R. D. Piner, K. A. Kohlhaas, A. Kleinhammes, Y. Jia, Y. Wu, S. T. Nguyen and R. S. Ruoff, *Carbon*, 2007, **45**, 1558–1565.

146 M. Khazaei, M. Arai, T. Sasaki, C.-Y. Chung, N. S. Venkataramanan, M. Estili, Y. Sakka and Y. Kawazoe, *Adv. Funct. Mater.*, 2013, **23**, 2185–2192.

147 M. Khazaei, A. Ranjbar, M. Arai, T. Sasaki and S. Yunoki, *J. Mater. Chem. C*, 2017, **5**, 2488–2503.

148 E. Pomerantseva and Y. Gogotsi, *Nat. Energy*, 2017, **2**, 17089.